

Dalton Transactions

An international journal of inorganic chemistry

Accepted Manuscript

This article can be cited before page numbers have been issued, to do this please use: Z. Zhang, J. Kano, S. MORITA, H. Shimokawa and M. Osada, *Dalton Trans.*, 2026, DOI: 10.1039/D5DT03086B.



This is an Accepted Manuscript, which has been through the Royal Society of Chemistry peer review process and has been accepted for publication.

Accepted Manuscripts are published online shortly after acceptance, before technical editing, formatting and proof reading. Using this free service, authors can make their results available to the community, in citable form, before we publish the edited article. We will replace this Accepted Manuscript with the edited and formatted Advance Article as soon as it is available.

You can find more information about Accepted Manuscripts in the [Information for Authors](#).

Please note that technical editing may introduce minor changes to the text and/or graphics, which may alter content. The journal's standard [Terms & Conditions](#) and the [Ethical guidelines](#) still apply. In no event shall the Royal Society of Chemistry be held responsible for any errors or omissions in this Accepted Manuscript or any consequences arising from the use of any information it contains.

Cite this: DOI: 00.0000/xxxxxxxxxx

Unraveling the structural features of Dion–Jacobson–type layered perovskite-related material $\text{HCa}_2\text{Nb}_3\text{O}_{10} \cdot 1.5\text{H}_2\text{O}$ Zihao Zhang^a, Jun Kano^{*a}, Shu Morita^b, Hiromu Shimokawa^a, Minoru Osada^c

Received Date

Accepted Date

DOI: 00.0000/xxxxxxxxxx

Hydrated layered oxides are widely encountered, yet the presence of disordered interlayer water often complicates crystal structure determination from laboratory X-ray diffraction. Here, we report the crystal structure of the Dion–Jacobson–type layered perovskite-related material $\text{HCa}_2\text{Nb}_3\text{O}_{10} \cdot 1.5\text{H}_2\text{O}$, solved from synchrotron X-ray diffraction data by combining direct methods in reciprocal space, Le Bail whole-pattern fitting, and Rietveld refinement. The hydrate crystallizes in a tetragonal structure with space group $P4_22_12$ ($a = 7.7070(5) \text{ \AA}$, $c = 32.4870(3) \text{ \AA}$). Incorporation of partially occupied interlayer water–oxygen sites on the (110) plane at $z = 0$ and $1/2$ successfully reproduces the low-angle $00l$ reflections while preserving the $\text{Ca}_2\text{Nb}_3\text{O}_{10}$ framework. The resulting crystallographic model explicitly resolves the arrangement of interlayer water molecules and provides a robust structural foundation for band-structure calculations as well as for the rational design of hydration-controlled intercalation, exfoliation, and composite materials based on layered perovskite-related materials.

1 Introduction

2 Layered perovskite-related materials have attracted increasing at-
3 tention for electronic and energy applications, owing to their
4 structurally tunable frameworks and rich physical properties.^{1–4}
5 Among them, Dion–Jacobson (DJ)–type oxides consist of nega-
6 tively charged perovskite-derived slabs separated by exchange-
7 able interlayer cations, giving rise to pronounced structural
8 anisotropy and exceptional ion-exchange and intercalation capa-
9 bilities. These features make DJ-type oxides versatile platforms
10 for the construction of composite materials and two-dimensional
11 (2D) nanosheets. Through interlayer ion exchange, intercalation,
12 and exfoliation processes, extensive structural design strategies
13 have been developed, enabling the transformation of bulk layered
14 oxides into 2D nanosheets, thin films, superlattices, and func-
15 tional hybrid materials.⁵ Within this material family, protonated
16 DJ-type oxides such as $\text{HCa}_2\text{Nb}_3\text{O}_{10}$ (HCNO) and their hydrated
17 derivatives have been extensively investigated as photocatalysts
18 for hydrogen evolution from water under ultraviolet irradiation.⁶

19 Previous studies have demonstrated that the photocatalytic activ-
20 ity of HCNO hydrates is highly sensitive to the hydration state
21 and the nature of interlayer species. Interlayer $\text{H}_2\text{O}/\text{H}_3\text{O}^+$
22 ions are thought to facilitate proton conduction while modulat-
23 ing interlayer spacing and charge-carrier migration through hydro-
24 gen-bond networks and electrostatic screening effects, thereby influ-
25 encing the overall photocatalytic performance.⁷ Moreover, hy-
26 drated and protonated DJ-type oxides serve as essential precu-
27 sors for further intercalation of organic amines, incorporation of
28 macromolecular species, and immobilization of metal nanoparti-
29 cles, with interlayer water playing a critical role in ion-exchange
30 reactions, osmotic swelling, and exfoliation behavior in aqueous
31 media.^{5,8} Despite their functional importance, detailed structural
32 information on DJ-type hydrates, including HCNO hydrates, re-
33 mains scarce. Most previous studies have relied on laboratory
34 X-ray diffraction and thermal analysis to derive average lattice
35 parameters and estimate water content. Consequently, the pre-
36 cise crystallographic locations of interlayer water molecules, their
37 coordination environments, and their spatial relationship with
38 the framework of the perovskite-derived slabs have not been sys-
39 tematically elucidated.⁷ This lack of structural insight hampers a
40 fundamental understanding of how hydration governs the phys-
41 ical and chemical properties of DJ-type oxides and limits ratio-
42 nal structural design for subsequent intercalation and exfolia-
43 tion processes. In this study, we focus on the hydrated phase
44 $\text{HCa}_2\text{Nb}_3\text{O}_{10} \cdot 1.5\text{H}_2\text{O}$ as a representative DJ-type hydrate, whose
45 hydration stoichiometry was established by thermogravimetric

^a Faculty of Environmental, Life, Natural Science and Technology, Okayama University, Okayama 700-8530, Japan. E-mail: kano-j@cc.okayama-u.ac.jp

^b Institute of Materials and Systems for Sustainability (IMaSS), Nagoya University, Nagoya 464-8601, Japan.

^c Department of Materials Chemistry and Institute of Materials and Systems for Sustainability (IMaSS), Nagoya University, Nagoya 464-8601, Japan; Research Institute for Quantum and Chemical Innovation, Institutes of Innovation for Future Society, Nagoya University, Nagoya 464-8601, Japan.



analysis (TGA) in early studies and has been consistently reported in subsequent work.⁹ Single-phase samples were synthesized by carefully controlling the proton-exchange and hydration conditions, and their crystal structures were refined using synchrotron X-ray diffraction (SR-XRD). Based on these data, we establish a reliable crystallographic model that explicitly resolves the arrangement of interlayer water molecules and interlayer cations. This structural model provides a robust crystallographic foundation for understanding hydration-induced functionalities in DJ-type oxides and offers a structural basis for future studies on intercalation chemistry, exfoliation into nanosheets, and the design of advanced composite materials.

2 Analytical procedure

The HCNO hydrate ($\text{HCa}_2\text{Nb}_3\text{O}_{10} \cdot 1.5\text{H}_2\text{O}$) was obtained by proton exchange of $\text{KCa}_2\text{Nb}_3\text{O}_{10}$ (KCNO) followed by hydration, and the dehydrated (non-hydrated) HCNO phase ($\text{HCa}_2\text{Nb}_3\text{O}_{10}$) was obtained by drying the hydrate. The detailed procedure is described in our previous work.¹⁰ In that study, the crystal structures of the precursor KCNO and the dehydrated (obtained by dry process) HCNO phase were determined by Rietveld refinement of SR-XRD data and were assigned to the monoclinic space group $P2_1/m$ and the tetragonal space group $P4_22_12$, respectively, with complete atomic positional and displacement parameters reported there. In this study, we focus on the hydrated HCNO. SR-XRD patterns were collected with a photon energy of 15.50 keV at Beamline BL5S2, Aichi Synchrotron Radiation Center. Diffraction-pattern indexing and direct methods in reciprocal space for structure solution as a probabilistic space-group search were carried out with EXPO2014, which ranks candidate space groups using normalized-intensity statistics and extinction-symbol analysis.¹¹ To refine the tetragonal unit-cell parameters and obtain integrated reflection intensities for checking extinction conditions, a Le Bail whole-pattern fit in $P4/mmm$ was performed using the GSAS-II program.¹² These results, together with the EXPO2014 space-group search, provided the basis for subsequent Rietveld refinements using RIETAN-FP.¹³

3 Results and Discussion

Fig. 1a shows the SR-XRD pattern of HCNO hydrate. For comparison, the patterns of dehydrated HCNO and KCNO are shown in Figs. 1b and c, respectively. Although our previous study successfully refined the structures of KCNO and dehydrated HCNO by the Rietveld method, all of the patterns are presented here with Le Bail whole-pattern fitting in order to clarify the structural evolution from the parent KCNO phase through protonation and subsequent dehydration. The precursor KCNO was previously determined to adopt the monoclinic space group $P2_1/m$, whereas dehydrated HCNO adopts the tetragonal space group $P4_22_12$.¹⁰ HCNO hydrate can likewise be indexed using a tetragonal cell, which is here described in $P4/mmm$. The diffraction patterns show that all samples show practically a single phase, with all reflections assignable to the layered perovskite phase and no detectable im-

purity peaks. KCNO, which is the parent material of HCNO, serves as the precursor reference, whereas comparison between dehydrated HCNO and HCNO hydrate clarifies the structural changes associated with hydration. Comparison of the lattice parameters shows that hydration mainly increases the lattice parameter along the stacking direction, with only a minimal change in the in-plane parameter. The elongation of the c -axis upon hydration may reflect not only an expansion of the interlayer region but also hydration-related effects on the $\text{Ca}_2\text{Nb}_3\text{O}_{10}$ framework. Thus, the observed increase in the c -axis lattice parameter should not be interpreted simply as the geometric size of an inserted water molecule, because the crystallographic c parameter also includes the thickness and subtle relaxation of the $\text{Ca}_2\text{Nb}_3\text{O}_{10}$ framework. This interpretation is consistent with the systematic shift of re-

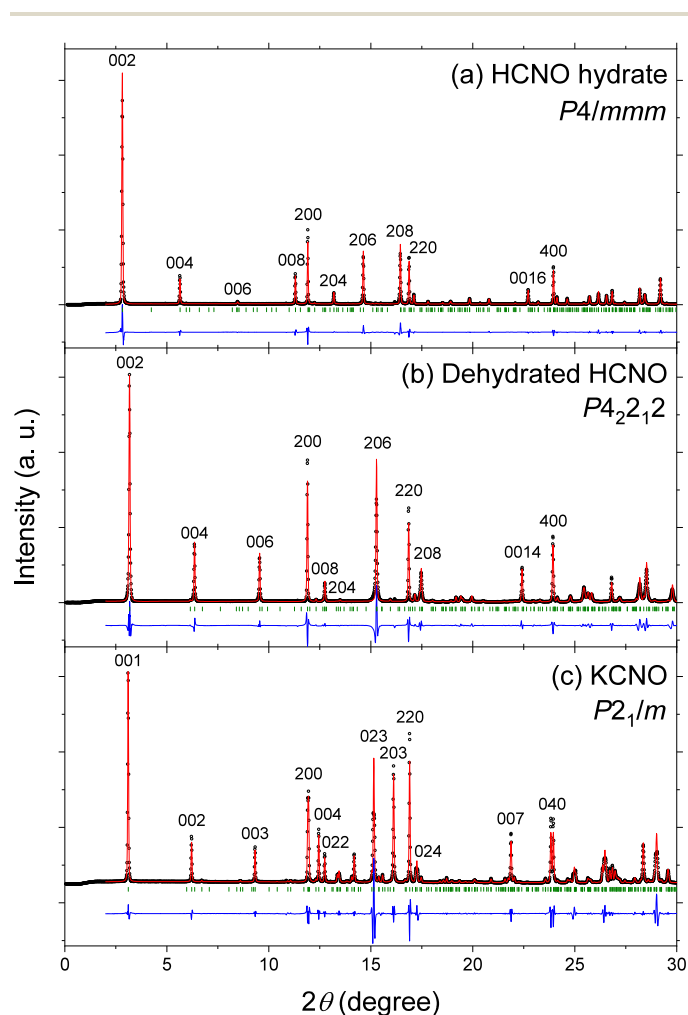


Fig. 1 SR-XRD patterns of (a) HCNO hydrate, (b) dehydrated HCNO, and (c) KCNO. The observed data are presented as open circles, together with the simulated (red lines) and difference (blue lines) patterns obtained by the Le Bail method installed in the GSAS-II program. The vertical green lines indicate the reflection positions. Reflections indexed by the Le Bail method are labeled with hkl . The refined lattice parameters are as follows: (a) HCNO hydrate with the tetragonal space group $P4/mmm$, $a = 7.7101(11)$, $c = 32.4990(4)$ Å, $R_{\text{wp}} = 12.64$, and $S = 2.23$; (b) dehydrated HCNO with $P4_22_12$, $a = 7.7133(13)$, $c = 28.7965(5)$ Å, $R_{\text{wp}} = 17.40$, and $S = 2.29$; and (c) KCNO with $P2_1/m$, $a = 7.7494(2)$, $b = 7.7110(14)$, $c = 14.8832(5)$ Å, $\beta = 97.442(16)^\circ$, $R_{\text{wp}} = 15.23$, and $S = 1.64$.

1 flections with non-zero l indices toward lower 2θ , whereas the
2 $hk0$ reflections remain nearly unchanged. The overall correspon-
3 dence between the major reflections of HCNO hydrate and dehy-
4 drated HCNO suggests that the basic layered framework is largely
5 retained upon hydration, with the principal structural change oc-
6 ccurring along the stacking direction. For direct structural compar-
7 ison with HCNO hydrate, the fractional atomic coordinates and
8 isotropic displacement parameters of dehydrated HCNO are also
9 provided in Table S1 of the ESI†.

10 For the assignment of the space group of HCNO hydrate,
11 diffraction pattern indexing and space group candidate search-
12 ing were performed using EXPO2014 software after peak-shape
13 modelling and background subtraction.¹¹ The indexing figures of
14 merit indicated that the crystal belongs to the tetragonal crys-
15 tal system, and the extinction-symbol analysis of the normalized
16 intensities indicated that its Bravais lattice is of primitive (P -
17 type).^{14,15} Subsequently, a Le Bail whole-pattern decomposition
18 was performed in the tetragonal space group $P4/mmm$, which has
19 no systematic extinctions, to refine the unit-cell metrics and pro-
20 file parameters. To assess the possible presence of a superstruc-
21 ture, peak positions were compared on the basis of whole-pattern
22 Le Bail fitting using several candidate cells derived from the par-
23 ent tetragonal lattice. Smaller trial cells, including $a \times a \times c$ and
24 $\sqrt{2}a \times \sqrt{2}a \times \sqrt{2}c$, were also examined, but they failed to repro-
25 duce the additional weak reflections. Among the tested models,
26 the $2a \times 2a \times 2c$ supercell provided the best overall match (see
27 Fig. S1, ESI†). Using this refined cell, the space group determi-
28 nation module of EXPO2014 evaluated candidate extinction sym-
29 bols based on systematic absences and the statistics of normal-
30 ized intensities. Among the tetragonal space groups proposed
31 by EXPO2014, $P4_22_12$ and its minimal supergroup $P4_2/nbc$ re-
32 ceived the highest scores. Other high-ranking candidates were
33 likewise P -type tetragonal space groups with $P4_2$ -derived sym-
34 metry, which are supergroups of $P4_22_12$ in the group-subgroup
35 hierarchy, reinforcing the above assignment of a P -type tetrago-
36 nal lattice. According to the group-subgroup relations, $P4_22_12$
37 can be obtained from $P4_2/nbc$ via the maximal-subgroup chain
38 $P4_2/nbc \rightarrow P4_22_12 \rightarrow P4_22_12$ (overall subgroup index 4), indicating
39 a simple symmetry-lowering relationship between the two candi-
40 date space groups. To further verify these candidate results, we
41 compared the integrated reflection intensities obtained from a Le
42 Bail fit in $P4/mmm$ with the systematic-absence conditions for the
43 candidates. No significant intensity above background was de-
44 tected for $00l$ with l odd or for $h00$ with h odd, and $hk0$ reflections
45 satisfied $h + k = 2n$. These observations are consistent with the
46 extinction requirements of $P4_2/nbc$ and $P4_22_12$.

47 Based on the space group candidates obtained by EXPO2014,
48 together with the extinction verification from integrated intensi-
49 ties of a Le Bail whole-pattern decomposition, Rietveld refine-
50 ment was carried out by using RIETAN-FP for $P4/mmm$, $P4_2/nbc$,
51 and $P4_22_12$.¹³ A modified split pseudo-Voigt function with a
52 partial profile relaxation was used as the profile function.¹⁶ Struc-
53 tural models for HCNO hydrate were constructed based on the
54 layer-stacking pattern and cation positions previously established
55 for HCNO.¹⁰ In these models, interlayer water species were not
56 modelled at this stage; such NbO_6 octahedral framework-only

configuration will hereafter be referred to as “framework-only
57 model”. The resulting models, which contained only the NbO_6
58 octahedral framework, were refined in $P4/mmm$, $P4_2/nbc$ and
59 $P4_22_12$ using the same unit-cell and profile parameters. Note that,
60 due to the plate-like particle shape of the HCNO hydrate,
61 preferred orientation had to be considered, even though the SR-
62 XRD measurements were performed while rotating the sample in-
63 side the capillary. A partial profile relaxation was applied in the
64 Rietveld refinement, which improved the fit for the reflections in
65 the low- 2θ region.

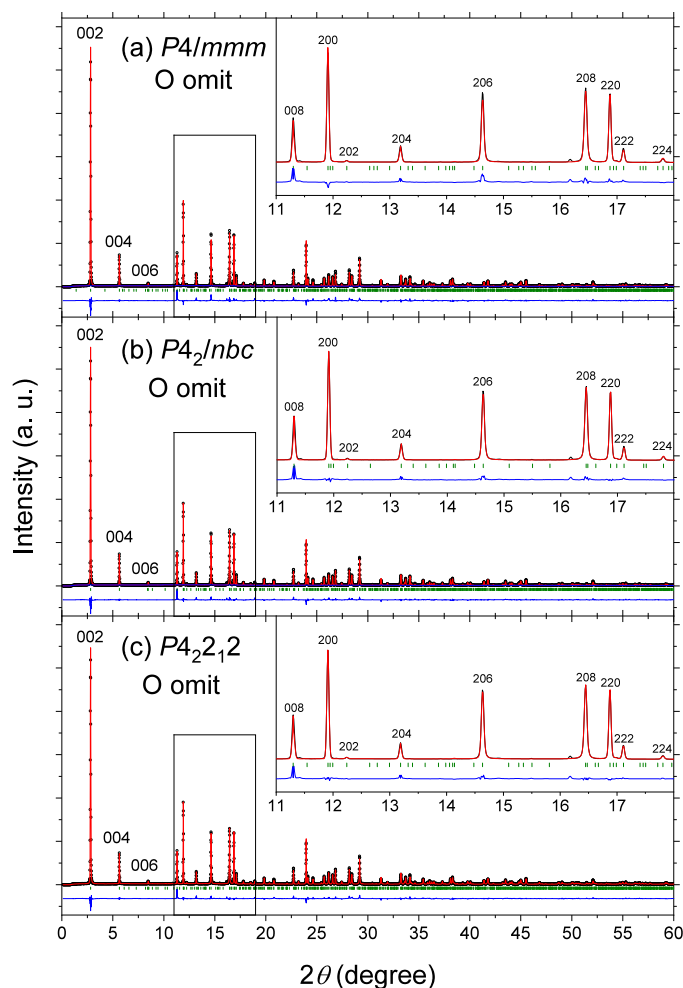


Fig. 2 SR-XRD patterns and fitting results for HCNO hydrate using
framework-only models in which interlayer water oxygen atoms were omi-
ted (O omit). The observed data are presented as open circles with
simulated (red lines) and difference (blue lines) patterns by the Rietveld
refinement. The vertical green lines represent the positions of the reflec-
tions. The insets show the reflections located in the low- 2θ regions on a
magnified scale. Analyzed for (a) $P4/mmm$, (b) $P4_2/nbc$, (c) $P4_22_12$. For
 $P4/mmm$, $a = 7.7064(8)$, $c = 32.4864(5)$ Å; $R_{wp} = 12.07$; and $S = 2.15$. For
 $P4_2/nbc$, $a = 7.7063(7)$, $c = 32.4869(4)$ Å; $R_{wp} = 10.06$; and $S = 1.79$. For
 $P4_22_12$, $a = 7.7071(7)$, $c = 32.4883(4)$ Å; $R_{wp} = 9.88$; and $S = 1.76$.

Fig. 2 shows the result of the Rietveld refinement for the
 $P4/mmm$, $P4_2/nbc$, and $P4_22_12$ space groups. The reliability indi-
ces show a clear improvement from $P4/mmm$ to $P4_2/nbc$ and
 $P4_22_12$, with the lowest R_{wp} and S values obtained for $P4_22_12$, in-
dicating that the lower-symmetry models reproduce the observed



intensity distribution more accurately under comparable refinement conditions. Clear differences among the three refinements are observed for reflections that are sensitive to distortions of the NbO_6 octahedral framework, including subtle displacements of the Ca cations within the $\text{Ca}_2\text{Nb}_3\text{O}_{10}$ framework. For the low-angle $00l$ reflections, the difference curves reveal larger deviations in $P4/mmm$ than in $P4_2/nbc$ and $P4_22_12$, with $P4_22_12$ giving the lowest residuals among the three models. A similar tendency is observed for several reflections shown in the low- 2θ region, such as 200, 206, and 208, where the calculated intensities for $P4/mmm$ deviate more strongly from the observed ones than in the refinements using $P4_2/nbc$ or $P4_22_12$. These differences are consistent with symmetry lowering from $P4/mmm$ to $P4_2/nbc$ and $P4_22_12$, which allows additional distortion modes of the NbO_6 octahedral framework that are incompatible with $P4/mmm$. Nevertheless, even in $P4_22_12$ noticeable deviations remain for reflections in the low- 2θ region, particularly the $00l$ series, indicating that a model containing only the NbO_6 octahedral framework does not fully account for the observed scattering intensities. Given that HCNO hydrate has the composition $\text{HCa}_2\text{Nb}_3\text{O}_{10} \cdot 1.5\text{H}_2\text{O}$, this remaining discrepancy can be derived from a scattering contribution from interlayer water molecules that is not included in the present framework-only model.

To resolve the remaining discrepancies in the framework without interlayer water molecules, further Rietveld refinements were carried out, introducing crystallization water into the interlayer region of the model. Because hydrogen atoms scatter X-rays only very weakly and their coordinates cannot be determined reliably from powder data,¹⁷ only the oxygen atoms of the interlayer water molecules were refined as crystallographic sites in the model, and the associated hydrogen atoms were not included in the refinement.¹⁸ In related layered perovskite oxides, distinct hydration arrangements have been reported depending on the interlayer species and the degree of hydration; a bilayer-hydrate model accommodating interlayer K^+ ions solvated by two water layers has been proposed for restacked $\text{KCa}_2\text{Nb}_3\text{O}_{10} \cdot 1.3\text{H}_2\text{O}$.¹⁹ Such a bilayer arrangement is typically associated with the presence of solvated interlayer alkali cations and may therefore not be directly transferable to the present protonated hydrate. More specific water orientations have also been discussed for stoichiometrically hydrated Ruddlesden–Popper–type oxides, where low-temperature neutron powder diffraction analysis revealed intact H_2O in a vertical “pillared” orientation hydrogen-bonded to apical oxygen atoms.²⁰ However, because hydrogen atoms are poor X-ray scatterers and their positions are difficult to determine reliably from X-ray powder diffraction data, the present SR-XRD refinement primarily constrains the average positions/occupancies of the interlayer oxygen sites, leaving the H_2O orientation undetermined. Given the limited sensitivity of X-ray powder data to hydrogen and the likelihood of orientational/disorder effects, we adopted an average-structure description guided by previous neutron-diffraction-based analyses of hydrated layered perovskite oxides, in which interlayer $\text{H}_2\text{O}/\text{H}_3\text{O}^+$ species statistically occupy sites around the body-center of the interlayer cavity defined by apical oxygens of adjacent NbO_6 octahedral layers.²¹ Accordingly, the water molecules were assumed to reside around the

mid-planes of the interlayer between neighbouring NbO_6 octahedral layers, corresponding to the planes $z = 0$ and $1/2$ in the unit cell. We compared special positions with multiplicities of 2 and 4 against two symmetry-equivalent sets of multiplicity 8 near $z = 0$ and $1/2$, refining a partial occupancy for the latter so that the total interlayer water content matches the nominal stoichiometry of $\text{HCa}_2\text{Nb}_3\text{O}_{10} \cdot 1.5\text{H}_2\text{O}$; the latter gave lower residuals and was therefore adopted. For schematic visualization of hydrogen bonding, the interlayer H sites were placed at fixed nominal positions slightly displaced from the interlayer water planes, with $z = 0.05$. Because the present SR-XRD data cannot constrain the precise coordinates of the H sites, these H coordinates were not refined and should not be interpreted as experimentally determined H positions. All other refinement parameters and the NbO_6 octahedral framework model were kept identical to those used in the framework-only refinements described above.

Fig. 3 shows the Rietveld refinement results obtained using models that include partially occupied interlayer water-oxygen sites (O_w) for the $P4/mmm$, $P4_2/nbc$ and $P4_22_12$ space groups. Compared with the framework-only refinements in Fig. 2, the agreement factors are further reduced for all three space groups, with $P4_22_12$ again giving the lowest values ($R_{\text{wp}} = 7.76$ and $S = 1.38$). Hamilton’s R -factor ratio test confirms that the improvements obtained with the lower-symmetry models are statistically significant in both the framework-only refinements and the refinements including interlayer water-oxygen sites (Table S2 and Fig. S2, ESI†).²² In addition, the difference curves around the low-angle reflections become noticeably flatter for all three models, especially for the $00l$ series. The deviations around the 002 and 008 peaks that remained in the framework-only model are largely reduced once interlayer water is included in the refinement, and the higher- 2θ region also shows smoother difference curves. This indicates that introducing interlayer water improves the overall fit to the diffraction pattern. For $P4_22_12$ in particular, the difference curve is basically flat over the whole 2θ range, apart from a small residual at the intense 002 reflection; no other significant residuals are observed. Although the differences between the three calculated profiles in Fig. 3 are small in appearance, the Rietveld agreement factors still favour $P4_22_12$ over $P4_2/nbc$ and $P4/mmm$, in accord with the EXPO2014 space group analysis and with the framework-only refinements in Fig. 2. On this basis, the space group of HCNO hydrate was determined to be $P4_22_12$ as the most appropriate description of HCNO hydrate. Fig. 4, drawn using VESTA software,²³ shows the refined crystal structure with the $P4_22_12$ space group. The positional disorder of this interlayer water was represented by partially occupied O sites in these planes. The fractional coordinates and isotropic atomic displacement parameters for HCNO hydrate are listed in Table 1, and the unit cell parameters are as follows: $a = 7.7070(5)\text{Å}$, $c = 32.4870(3)\text{Å}$, and $Z = 8$. Notably, the increase in the c -axis lattice parameter is attributed not only to the introduction of intercalated water, which slightly increases the interlayer spacing relative to non-hydrated $\text{HCa}_2\text{Nb}_3\text{O}_{10}$, but also to a subtle influence of the intercalated water on the NbO_6 octahedral framework.

This structural model also raises the question of the appropri-

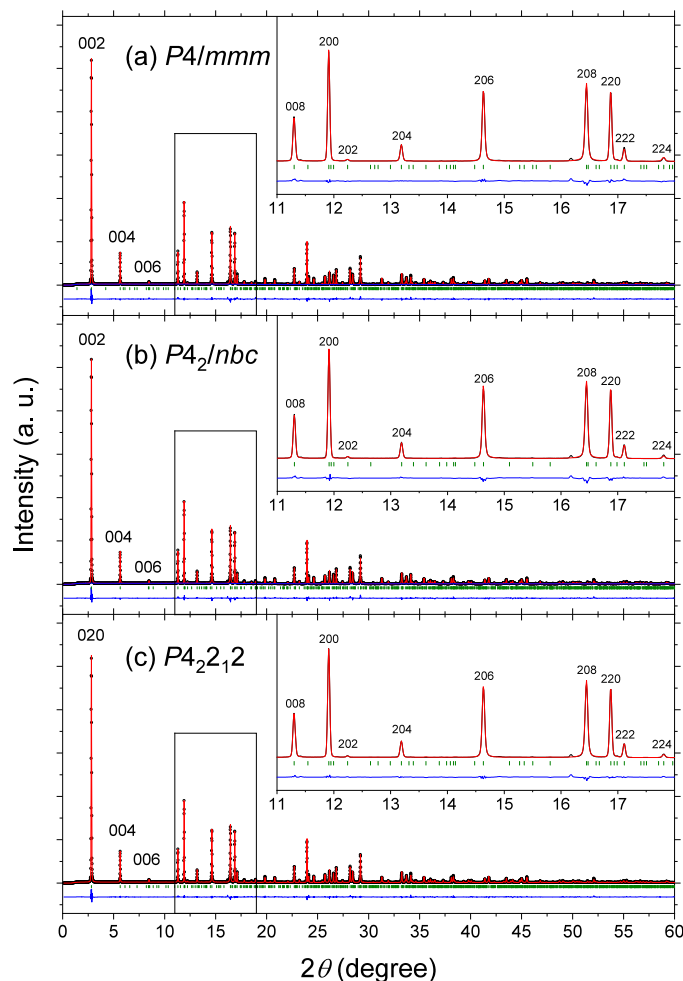


Fig. 3 SR-XRD patterns and fitting results for HCNO hydrate using models including interlayer water-oxygen sites. The observed data are presented as open circles with simulated (red lines) and difference (blue lines) patterns by the Rietveld refinement. The vertical green lines represent the positions of the reflections. The insets show the reflections located in the low- 2θ regions on a magnified scale. Analyzed for (a) $P4/mmm$, (b) $P4_2/nbc$, (c) $P4_22_12$. For $P4/mmm$, $a = 7.7073(6)$, $c = 32.4849(3)$ Å; $R_{wp} = 9.50$; and $S = 1.69$. For $P4_2/nbc$, $a = 7.7063(6)$, $c = 32.4846(3)$ Å; $R_{wp} = 8.46$; and $S = 1.51$. For $P4_22_12$, $a = 7.7070(5)$, $c = 32.4870(3)$ Å; $R_{wp} = 7.76$; and $S = 1.38$.

1 ate hydration stoichiometry for the refinement. For the refine-
 2 ments including O_w , the hydration stoichiometry of HCNO was
 3 also evaluated. Jacobson first reported that HCNO incorporates
 4 $1.5H_2O$ upon protonation of KCNO, with the water content deter-
 5 mined by TGA.⁹ Although many subsequent studies have re-
 6 ported values consistent with this result,²⁴ larger values (e.g., 1.6
 7 or ca. 1.9) have also been reported.^{7,25} We therefore examined
 8 the sensitivity of the refinement to the occupancy of O_w . Trial
 9 refinements in which the O_w occupancy was varied showed only
 10 a shallow minimum in R_{wp} as a function of occupancy (Fig. S3,
 11 ESI†), indicating limited sensitivity of the data to this parameter.
 12 To maintain consistency and reliability, the O_w occupancy was
 13 fixed in the final refinements at the nominal value correspond-
 14 ing to $HCa_2Nb_3O_{10} \cdot 1.5H_2O$, following the nominal composition
 15 previously reported by Jacobson.

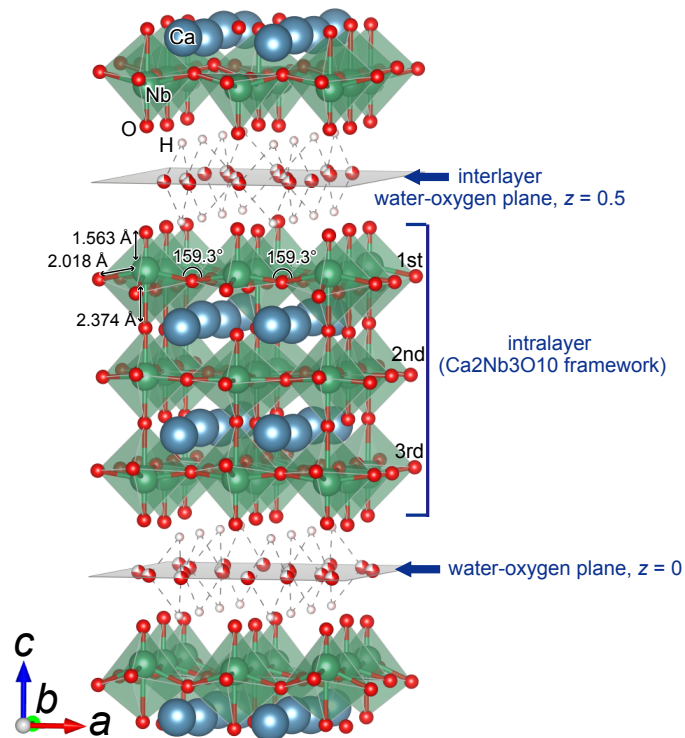


Fig. 4 Layer-stacking model of $HCa_2Nb_3O_{10} \cdot 1.5H_2O$ refined in space group $P4_22_12$, viewed along the b axis. Three NbO_6 octahedral layers and the interlayer water-oxygen planes at $z = 0$ and $1/2$ are shown; green octahedra represent NbO_6 units and blue spheres denote Ca atoms, while the white spheres labelled H indicate the protons in HCNO used schematically to illustrate hydrogen bonding. The crystal structures were drawn with VESTA.²³

To further evaluate the local coordination geometry, we exam-
 1 1 ined the bond-valence sums (BVSs) for the refined structure (see
 1 2 Table 1). The relatively high BVS at the Nb2 site (approximately
 1 3 6.5) is mainly attributable to the presence of two particularly
 1 4 short Nb2–O3 bonds. Because bond valence depends exponen-
 1 5 tially on bond length, such local shortening can lead to a signifi-
 1 6 cant increase in the BVS at a specific site. Therefore, this result
 1 7 should be understood as a local feature of the distorted NbO_6
 1 8 octahedron rather than as evidence against the overall structural
 1 9 model. This tendency may also be qualitatively consistent with
 2 0 the covalent character of the Nb–O bonds. The resulting struc-
 2 1 tural model is essentially consistent with earlier descriptions of
 2 2 HCNO, and the intercalated water did not induce any major rear-
 2 3 rangement of the $Ca_2Nb_3O_{10}$ framework.

4 Conclusion

In this work, synchrotron powder X-ray diffraction combined with
 31 Rietveld analysis establishes $P4_22_12$ as the most appropriate space
 32 group for $HCa_2Nb_3O_{10} \cdot 1.5H_2O$. Introducing statistically dis-
 33 tributed interlayer water-oxygen sites is essential to reproduce
 34 the low-angle $00l$ intensities, while the $Ca_2Nb_3O_{10}$ framework
 35 remains essentially unchanged relative to the dried HCNO phase.
 36 Our crystallographic model will contribute toward a reliable basis
 37 for subsequent electronic-structure calculations and related theo-
 38



Table 1 The crystallographic data and structural parameters provided by Rietveld analysis. Fractional coordinates and isotropic atomic displacement parameters of $\text{HCa}_2\text{Nb}_3\text{O}_{10} \cdot 1.5\text{H}_2\text{O}$ with space group $P4_22_12$. Here, g and B denote the site-occupation factor (occupancy) and the atomic displacement parameter of each crystallographic site, respectively. Selected bond valence sum (BVS) values for the framework Nb and O sites are also listed. The BVS values were calculated from the refined bond lengths using the bond-valence expression $V_i = \sum_j \exp[(R_{0j} - R_{ij})/b]$, and were evaluated within the $\text{Ca}_2\text{Nb}_3\text{O}_{10}$ framework only.

$\text{HCa}_2\text{Nb}_3\text{O}_{10} \cdot 1.5\text{H}_2\text{O}$ tetragonal $P4_22_12$
 $a = 7.7070(5)\text{Å}$, $c = 32.4870(3)\text{Å}$

Atom	Site	g	x	y	z	B (Å^2)	BVS
H1	8g	0.5	1/4	1/4	0.05 (fixed)	0 (fixed)	—
H2	8g	0.5	1/4	3/4	0.05 (fixed)	0 (fixed)	—
Ca1	8g	1	0.2509(16)	0.2535(16)	0.1837(2)	1.31(4)	—
Ca2	8g	1	0.2569(15)	0.7447(17)	0.1790(2)	1.31(-)	—
Nb1	4d	1	1/2	0	0.1151(10)	0.36(3)	5.62
Nb2	4d	1	1/2	0	0.2497(15)	0.36(-)	6.51
Nb3	4d	1	1/2	0	0.3800(12)	0.36(-)	5.20
Nb4	4c	1	0	0	0.1218(15)	0.77(4)	4.70
Nb5	4c	1	0	0	0.2485(19)	0.77(-)	5.26
Nb6	4c	1	0	0	0.3816(15)	0.77(-)	5.25
O _w 1	8g	0.75	0.5732(6)	0.2017(5)	0	11.81(105)	—
O _w 2	8g	0.75	0.3140(6)	0.1385(5)	0	11.81(-)	—
O1	8g	1	0.2411(6)	-0.0063(7)	0.3641(6)	1.53(12)	2.20
O2	8g	1	-0.0094(6)	0.2436(6)	0.3726(6)	1.53(-)	2.16
O3	8g	1	0.2755(2)	0.0000(4)	0.2451(6)	1.53(-)	2.45
O4	8g	1	-0.0777(14)	0.2532(5)	0.2481(9)	1.53(-)	1.90
O5	8g	1	0.0104(6)	0.2471(5)	0.1300(7)	1.53(-)	2.19
O6	8g	1	0.2553(5)	0.0013(7)	0.1420(6)	1.53(-)	2.01
O7	4d	1	1/2	0	0.0670(13)	5.06(65)	2.56
O8	4d	1	0	1/2	0.0682(15)	5.06(-)	1.84
O9	4d	1	1/2	0	0.3094(13)	5.06(-)	1.78
O10	4d	1	0	1/2	0.3119(14)	5.06(-)	1.57
O11	4c	1	0	0	0.0650(14)	4.40(60)	1.19
O12	4c	1	1/2	1/2	0.0612(12)	4.40(-)	1.15
O13	4c	1	0	0	0.3053(16)	4.40(-)	1.94
O14	4c	1	1/2	1/2	0.3053(16)	4.40(-)	2.26

$R_{\text{wp}} = 7.76$, $S = 1.38$

retical studies.

Author contributions

J.K. proposed the idea, and J. K. and Z.Z. supervised the entire project. S.M. and M.O. provided the synthesis procedure and technical support for sample preparation. Z.Z., S.M., and M.O. prepared the samples. J. K. performed the synchrotron powder X-ray diffraction measurements. Z.Z. carried out the diffraction analysis, including indexing, space-group determination, and Le Bail/Rietveld refinements, under the guidance of J.K. H.S. and Z.Z. evaluated the statistical significance of the refinements using Hamilton's R -factor ratio test. Z.Z. and J.K. interpreted the results. All the authors discussed the results of the study. Z.Z., J.K., S.M., and M.O. co-wrote the manuscript.

Conflicts of interest

The authors declare no competing interests.

Data availability

A data availability statement (DAS) is required to be submitted alongside all articles. Please read our full guidance on data availability statements for more details and examples of suitable statements you can use.

Acknowledgements

We thank Dr. Tomohiro Ikeda (Honda R&D Co., Ltd.) and Dr. Yuuki Nakanishi (Aichi Synchrotron Radiation Center) for technical assistance with the SR-XRD. This work was supported by the JSPS KAKENHI (Grants Nos. 20KK0330, 20H02609, 21H05015, 22K18976, 24K08247, and 25K22296) and JSPS Program for Forming Japan's Peak Research Universities (J-PEAKS, Grant No. JPJS00420230010).

References

- M. Osada and T. Sasaki, *Dalton Trans.*, 2018, **47**, 2841–2851.
- B.-W. Li, M. Osada, Y.-H. Kim, Y. Ebina, K. Akatsuka and T. Sasaki, *J. Am. Chem. Soc.*, 2017, **139**, 10868–10874.
- H.-J. Kim, S. Morita, K.-N. Byun, Y. Shi, T. Taniguchi, E. Yamamoto, M. Kobayashi, Y. Ebina, T. Sasaki and M. Osada, *Nano Lett.*, 2023, **23**, 3788–3795.
- S. Morita, D. Urushihara, K. Nishibashi, M. Kobayashi, E. Yamamoto, T. Asaka, H. Nakajima, S. Mori and M. Osada, *J. Am. Chem. Soc.*, 2024, **146**, 25221–25231.
- R. Uppuluri, A. S. Gupta, A. S. Rosas and T. E. Mallouk, *Chem. Soc. Rev.*, 2018, **47**, 2401–2430.
- S. Tasleem and M. Tahir, *Int. J. Hydrogen Energy*, 2020, **45**, 19078–19111.
- M. G. Shelyapina, O. I. Silyukov, E. A. Andronova, D. Y. Nefe-



- 1 dov, A. O. Antonenko, A. Missyul, S. A. Kurnosenko and I. A.
2 Zvereva, *Molecules*, 2021, **26**, 5943.
- 3 8 T. Sasaki and M. Watanabe, *J. Am. Chem. Soc.*, 1998, **120**,
4 4682–4689.
- 5 9 A. J. Jacobson, J. T. Lewandowski and J. W. Johnson, *J. Less-*
6 *Common Met.*, 1986, **116**, 137–146.
- 7 10 Z. Zhang, N. Oshime, Y. Hamasaki, M. Osada, S. Morita,
8 Y. Takaguchi, M. Yamagami, T. Okubo, K. Horigane, N. Ikeda,
9 T. Fujii, P. Gemeiner, P. Janolin, S. Hirose and J. Kano, *Elec-*
10 *tronic band structures of the Dion–Jacobson layered perovskite*
11 *KCa₂Nb₃O₁₀ and its protonated/exfoliated derivatives for the*
12 *design of photocatalysts*, Authorea Preprints, 2025, <https://doi.org/10.22541/au.175286046.61178722/v1>.
- 13 11 A. Altomare, C. Cuocci, C. Giacobozzo, A. Moliterni, R. Rizzi,
14 N. Corriero and A. Falcicchio, *J. Appl. Cryst.*, 2013, **46**, 1231–
15 1235.
- 16 12 B. H. Toby and R. B. V. Dreele, *J. Appl. Cryst.*, 2013, **46**, 544–
17 549.
- 18 13 F. Izumi and K. Momma, *Solid State Phenom.*, 2007, **130**, 15–
19 20.
- 20 14 A. Altomare, R. Caliendo, M. Camalli, C. Cuocci, C. Giacob-
- 21 *ozzo*, A. G. G. Moliterni and R. Rizzi, *J. Appl. Cryst.*, 2004, **37**,
22 1025–1028.
- 23 15 L. Palatinus and A. van der Lee, *J. Appl. Cryst.*, 2008, **41**, 975–
24 984.
- 25 16 F. Izumi, *J. Ceram. Soc. Jpn.*, 2003, **111**, 617–623.
- 26 17 M. Woińska, S. Grabowsky, P. M. Dominiak, K. Woźniak and
27 D. Jayatilaka, *Sci. Adv.*, 2016, **2**, e1600192.
- 28 18 K. A. Selevich, L. S. Ivashkevich, A. F. Selevich and A. S.
29 Lyakhov, *Russ. J. Inorg. Chem.*, 2002, **47**, 1533–1536.
- 30 19 Y. Chen, X. Zhao, H. Ma, S. Ma, G. Huang, Y. Makita, X. Bai
31 and X. Yang, *J. Solid State Chem.*, 2008, **181**, 1684–1694.
- 32 20 S. Liu, M. Avdeev, Y. Liu, M. R. Johnson and C. D. Ling, *Inorg.*
33 *Chem.*, 2016, **55**, 1403–1411.
- 34 21 S. Nishimoto, M. Matsuda, S. Harjo, A. Hoshikawa, T. Ishi-
35 gaki, T. Kamiyama and M. Miyake, *J. Solid State Chem.*, 2006,
36 **179**, 3308–3313.
- 37 22 W. C. Hamilton, *Acta Cryst.*, 1965, **18**, 502–510.
- 38 23 K. Momma and F. Izumi, *J. Appl. Cryst.*, 2011, **44**, 1272–1276.
- 39 24 V. V. Voytovich, S. A. Kurnosenko, O. I. Silyukov, I. A. Rodi-
40 onov, I. A. Minich and I. A. Zvereva, *Front. Chem.*, 2020, **8**,
41 300.
- 42 25 S. L. Guertin, E. A. Joseph, D. Montasserasadi and J. B. Wiley,
43 *J. Alloys Compd.*, 2015, **647**, 370–374.
- 44



View Article Online
DOI: 10.1039/D5DT03086B

The data that support the findings of this study are available from the corresponding author upon reasonable request. Crystallographic data for dehydrated HCNO ($\text{HCa}_2\text{Nb}_3\text{O}_{10}$) and hydrated one ($\text{HCa}_2\text{Nb}_3\text{O}_{10} \cdot 1.5\text{H}_2\text{O}$) have been deposited under deposition numbers 2504732 and 2556680, respectively, via the CCDC/FIZ Karlsruhe deposition service. Additional information, such as input files for calculations and scripts used for analysis, can be provided upon request.

